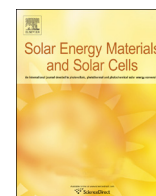




ELSEVIER

Contents lists available at ScienceDirect

## Solar Energy Materials &amp; Solar Cells

journal homepage: [www.elsevier.com/locate/solmat](http://www.elsevier.com/locate/solmat)

# Feasibility of submonolayer ZnTe/ZnCdSe quantum dots as intermediate band solar cell material system

S. Dhomkar<sup>a,b,\*</sup>, U. Manna<sup>c,1</sup>, L. Peng<sup>b,d</sup>, R. Moug<sup>d</sup>, I.C. Noyan<sup>c</sup>,  
M.C. Tamargo<sup>b,d</sup>, I.L. Kuskovsky<sup>a,b</sup>

<sup>a</sup> Department of Physics, Queens College of CUNY, Queens, NY 11367, USA

<sup>b</sup> The Graduate Center of CUNY, New York, NY 10016, USA

<sup>c</sup> Department of Applied Physics and Applied Mathematics, Columbia University, New York, NY 10027, USA

<sup>d</sup> Department of Chemistry, City College of CUNY, New York, NY 10031, USA

## ARTICLE INFO

### Article history:

Received 24 April 2013

Received in revised form

22 July 2013

Accepted 26 July 2013

### Keywords:

Intermediate band solar cell

Submonolayer

Type-II quantum dots

II–VI Semiconductors

## ABSTRACT

Intermediate band solar cells can potentially have an efficiency of  $\sim 63\%$  under full solar concentration, but the material systems investigated until now are far from optimum and are fraught with growth related issues such as low quantum dot densities, presence of wetting layers, and strain driven dislocations. Also, incorporation of type-I quantum dots increases carrier recombination rates, resulting in inferior performance. Here, we show that a novel material system with stacked type-II ZnTe-rich submonolayer QDs embedded in ZnCdSe has close to the optimal material parameters required for an intermediate band material system. We have grown structures comprising of as many as 150 layers of QDs that are formed without wetting layers and that have a valence band offset of  $\sim 0.8$  eV relative to the host with a bandgap of  $\sim 2.1$  eV. We demonstrate the possibility of intermediate band formation and subsequent absorption of below bandgap photons. Additionally, these structures are expected to have longer radiative lifetimes and to suppress Auger recombinations owing to their type-II nature.

© 2013 Elsevier B.V. All rights reserved.

## 1. Introduction

The intermediate band (IB) solar cell (SC) concept proposed by Luque and Martí in 1997 [1] provides a new insight into the conversion efficiencies of SCs, and offers a potential way to increase the limiting efficiency of an ideal single-gap SCs from 40.7% [2,3] to 63.2% [1,4,5] under full concentration. IB-SCs rely on multi-photon absorption with assistance of an IB lying in the mid-gap of an active material forming a SC [1,4,5]. Such an IB allows harvesting of photons with energy below the bandgap via transitions from the host semiconductor valence band (VB) to the IB and from the IB to the conduction band (CB) in addition to the conventional VB to CB transitions. The absorption of the additional IB assisted photons increases the photocurrent, while preserving the open circuit voltage, thus improving the external efficiency of the cell [1,4,5]. The formation of an IB by means of quantum dots (QDs) is considered to be the most practical and attractive approach to fabricate an efficient IB-SC [4,5].

In the QD based IB-SCs, either electron or hole confinement levels within the QDs give rise to an IB [4,5] depending on the

\* Corresponding author at: Department of Physics, Queens College of CUNY, Queens, NY 11367, USA. Tel.: +1 718 997 3370.

E-mail address: [sdhomkar@qc.cuny.edu](mailto:sdhomkar@qc.cuny.edu) (S. Dhomkar).

<sup>1</sup> Both these authors contributed equally to this work.

bandgaps and band-offsets of the constituent materials. The proof of concept has been successfully demonstrated in the type-I InAs/GaAs QDs [6,7] with the IB engineered out of electron confinement levels; moreover, the efficiencies obtained show significant improvements as compared to the reference GaAs cell when QDs are appropriately doped [8]. However, the main constraints that limit the performance of such IB-SCs are [4,5]: (i) the bandgaps of the proto-type InAs/GaAs QD SCs are far from the theoretically calculated optimal values for host bandgap ( $\sim 1.95$  eV) and the IB ( $\sim 0.71$  eV) [1,4,5], though some modifications have been proposed for the purpose of optimization [9,10]; (ii) an insufficient increase in the short circuit current because of relatively low absorption due to the small number of QD layers; relatively a few layers of QDs can be grown via the Stranski–Krastanov growth mode due to accumulation of strain and subsequent formation of dislocations [11]; (iii) a reduction of the open circuit voltage due to the existence of the wetting layers formed as a consequence of the Stranski–Krastanov growth; the presence of a wetting layers prevents the QDs to form well-separated confined states for electrons (or holes), resulting in a continuum of states following strong thermal escape, reducing the open circuit voltage; (iv) type-I QDs have both types of carriers spatially confined in the same volume, enhancing the probability of electron–hole scattering and recombination [12,13]. Here, we propose submonolayer type-II ZnTe-rich QDs embedded in a  $Zn_xCd_{1-x}Se$  ( $x \sim 0.51$ ) matrix as an IB

material and show the feasibility of such a system to address the above mentioned deficiencies of the proto-type QD based IB-SCs. The proposed structure is believed to possess the material parameters with the best possible match to those of an ideal IB-SC.

The  $\text{Zn}_x\text{Cd}_{1-x}\text{Se}$  alloy has a band gap of about 2.1 eV at room temperature [14], when grown lattice matched to InP, hence it can be used as a host material with a bandgap close to the ideal one. Also, ZnTe QDs having a VB offset of about 0.8 eV [15–17] relative to the  $\text{Zn}_{0.51}\text{Cd}_{0.49}\text{Se}$  can be used to engineer an optimum IB out of the hole confinement levels. To verify this assumption, we thus have grown submonolayer ZnTe/ZnCdSe multilayer QDs with as many as 150 periods by means of migration enhanced epitaxy (MEE). The submonolayer nature of these QDs and their growth mechanism allow them to form without the formation of the wetting layers. The multilayer nature of the vertically correlated ZnTe/ZnCdSe QDs is shown to manifest via the IB related absorption. Hence, incorporation of ZnTe/ZnCdSe submonolayer QDs in a practical device is expected to increase the short circuit current, while the formation of QDs without the wetting layer is expected to preserve the open circuit voltage. Moreover, the type-II nature of these heterostructures is also expected to suppress the non-radiative Auger [18] recombination as well as to improve the process of charge extraction [19]. In subsequent sections, we show that such a system indeed possesses ‘close-to-ideal’ material and physical properties and thus could lead to a practical efficient IB-SC.

## 2. Experimental

### 2.1. Growth

Three samples (referred hereon as A, B, and C) were grown epitaxially on (001) semi-insulating InP substrates with increasing Te content in a RIBER 2300P molecular beam epitaxy system. After the growth of the InGaAs and ZnCdSe buffer layers, multilayered structure of ZnTe-rich QDs within a ZnCdSe matrix was grown via MEE, by exposing the growing surface to alternate elements using a specific shutter sequence shown in Fig. 1(a). A ZnCdSe barrier (nominally 8 monolayers) was first grown, followed by the three identical cycles of sequential depositions of Zn and Te separated by 5 s of growth interruptions. The whole sequence of the growth of the ZnCdSe barrier and the ZnTe QDs was then repeated 150 times to achieve a multilayered structure as illustrated in Fig. 1(b). Details of the growth technique have been reported elsewhere [20]. The Te source temperatures for samples A, B, and C were 236 °C, 241 °C, and 250 °C respectively, which correspond to beam equivalent pressures of  $0.38 \times 10^{-7}$  Torr,  $0.63 \times 10^{-7}$  Torr, and  $1.2 \times 10^{-7}$  Torr respectively.

## 3. Characterization

Low temperature PL measurements were performed using a Janis Research closed cycle refrigerating system. The 351 nm emission line from an  $\text{Ar}^+$  laser was used as an excitation source and the excitation intensity was varied by over four orders of magnitude using neutral density filters. The PL was dispersed through a third stage of a TriVista SP2 500i triple monochromator and was detected by a thermoelectrically cooled charge coupled device camera. The HRXRD measurements were carried out at Beamline X20A at the National Synchrotron Light Source at the Brookhaven National Laboratory. All measurements were performed using monochromatic synchrotron radiation at 8 keV, with a double-crystal Ge (111) monochromator. To enhance the angular resolution, a Si (111) analyzer was placed in front of the detector.

The absorption measurements were done in an ARC closed cycle refrigerating system from 10 K to room temperature. A broad spectrum halogen lamp was used as a light source and the signal was collected using an Ocean Optics VIS–NIR spectrometer.

## 4. Results and discussion

The special epitaxial technique described in Section 2.1 enables sequential deposition of the elements in submonolayer quantities, which, combined with the short interruptions, gives rise to enhanced surface migration. The submonolayer ZnTe QDs are formed by continuous enlargement of Te isoelectronic centers via Volmer–Weber growth mode without the formation of a wetting layer, analogous to ZnTe/ZnSe QDs reported previously [21,22]. Hundreds of layers containing QDs can be grown by this technique, potentially giving a large number of QDs, all without wetting layers. An additional advantage of such a growth mechanism is that the dopants, for instance Nitrogen for p-type doping in this case, can be easily incorporated preferentially into the QDs [22,23], in order to create a ‘half-filled’ IB as required for the optimal performance of an IB-SC [7,8].

Low temperature PL was employed to investigate the type-II nature of these QD structures. Fig. 1(c) and inset of Fig. 1(c) show the PL spectra for all the three samples for maximum excitation intensity and three orders of magnitude of lower excitation intensity, respectively at 10 K. Fig. 1(d) shows the dependence of the PL peak positions on excitation intensity with the peak positions showing strong blue shifts with increasing excitation intensity for all samples. Such a strong shift is a characteristic feature of type-II band alignment [21,24,25], and it is caused by band bending [24] that effectively changes the overlap of wavefunctions of the photo-generated electrons and holes. The PL peak positions were also found to approximately follow the cube root dependence on the excitation intensities as shown by the dotted lines in Fig. 1(d) for the three samples, in agreement with the prediction for large type-II nanostructures [24,26]. The PL spectra shown in Fig. 1(c) also demonstrate that there is a significant red shift in the PL peak position in case of samples B and C, which have higher Te concentrations as compared to that of sample A. This red-shift in PL emission energy with increasing Te concentration can be attributed to the increase in size of QDs due to higher Te content. Since Te concentration directly relates to Te source temperature (or Te flux), one gets an effective way to control the IB position by varying Te flux during the growth.

To investigate the “below bandgap” absorption occurring due to the possible ZnTe QD-based IB, we performed optical absorption measurements with results shown in Fig. 2. The below bandgap absorption was found to manifest itself via small peaks as indicated by arrows in the absorption spectra shown in Fig. 2. The energy of the below bandgap absorption peaks nominally corresponds to the PL peaks of the spatially indirect excitons in this type-II material system (see Fig. 1(c)). The observation of below bandgap peaks in the absorption spectra in spite of their spatially indirect nature indicates formation of the IB made out of the hole energy levels (detailed discussion on the IB formation is presented below). Due to smaller thicknesses of the disc-like submonolayer ZnTe QDs, the hole confinement energy lies close to the ZnCdSe VB as indicated by the position of absorption peaks in Fig. 2. It also needs to be stressed that the below bandgap absorption was only moderately enhanced with the inclusion of ZnTe QDs because of the undoped nature of these samples. The below bandgap absorption can further be improved by creating a half-filled IB by introducing p-type dopant during MEE cycles [22,23] within the QDs. The absorption measurements also enabled us to calculate the modified band gaps of the ZnCdSe

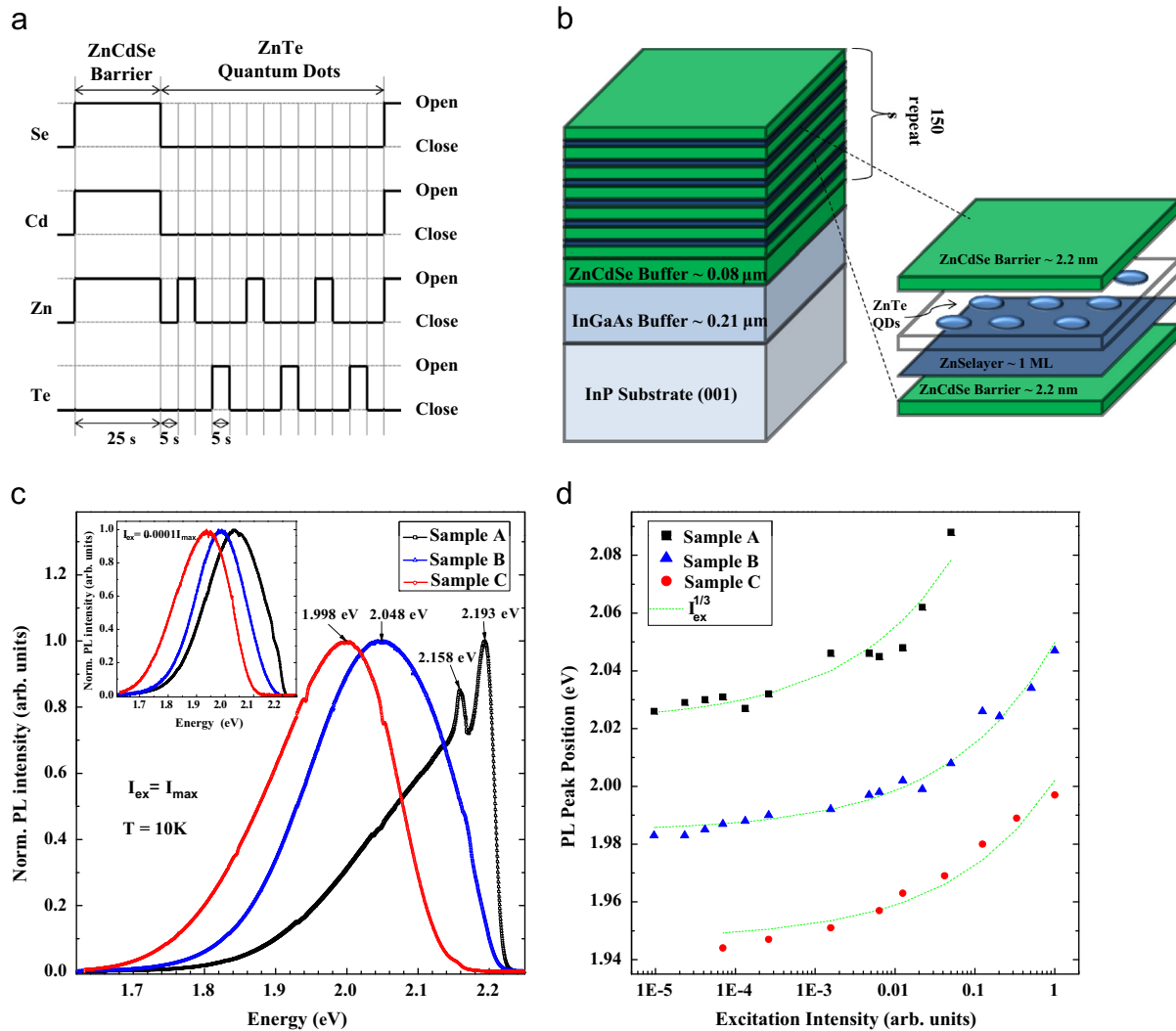


**Fig. 1.** Type-II ZnTe/ZnCdSe submonolayer QDs. (a) MEE shutter sequence used during the growth of the samples. (b) Schematic diagram of a typical ZnTe/ZnCdSe submonolayer QD SL. (c) The PL spectra of the three samples at 10 K, here  $I_{max}$  is the maximum excitation intensity. Inset: The PL spectra of the samples for four orders of magnitude lower excitation intensity. (d) The semilogarithmic plot of PL peak positions at 10 K for various excitation intensities, the dashed line is the result of fitting with the cube root of excitation intensity.

barriers due to minute Te diffusion. Upon calculating the absorption coefficient,  $\alpha$ , from the optical absorbance and the thickness of the superlattice (SL) structure estimated via HRXRD, the barrier band edges were obtained by plotting the  $(\alpha h\nu)^2$  as a function of photon energy ( $h\nu$ ) for all the three samples at room temperature as shown in the inset of Fig. 2.

In order to determine structural quality of the samples HRXRD studies were performed along symmetric (004) as well as asymmetric (224) reflections and the  $\omega$ - $2\theta$  curves along (004) orientation are shown in Fig. 3(a). Also, the structural parameters needed to calculate associated band gaps and band offsets of the ZnTe/ZnCdSe multilayer type-II QDs were obtained using these HRXRD measurements. The sharpness and intensities of the visible SL peaks up to fourth order for all the three samples are indicative of high crystalline quality of the samples. The in-plane lattice mismatches of the ZnCdSe buffer layers were calculated to be  $\sim 0.1\%$  for all the samples indicating that the ternary host alloys were almost lattice-matched to the InP substrate. The growth of lattice matched ZnCdSe barriers is especially important to avoid the formation of misfit dislocations, thereby eliminating the possibility of deleterious effects during the device operation. The compositions of the buffer layers (see Table 1), which are nominally same as that of the barrier layers, were calculated using the Bragg's law,

assuming that these layers were completely relaxed. The room temperature bandgaps of the ZnCdSe buffer layers, corresponding to the compositions, were then calculated to be  $\sim 2.1$  eV. The Te fractions in the barriers were then determined using calculated ZnCdSe buffer layer compositions and the absorption band edges of the corresponding barriers.

To confirm the calculated parameters of the multilayer structures obtained from HRXRD and absorption experiments,  $\omega$ - $2\theta$  curves along (004) direction were simulated by a commercially available BEDE RADS program based on Takagi and Taupin generalized dynamical theory. The simulation results are shown by the solid lines in Fig. 3(a) for all samples. For simulation purposes, we replaced the QD array by an effective layer of a thickness of about 0.07–0.10 nm with the same structure factor as that of the QDs and having some Se inclusion ( $\sim 40\%$ ) [27,28]. The results obtained from the simulations were found to be in excellent agreement with the parameters calculated by means of HRXRD and absorption measurements (Table 1). The simulations also revealed that the barriers are almost lattice matched to the substrate and a tensile mismatch is obtained due to the presence of 0.3 to 0.4 nm ( $\sim 1$  monolayer) thick fully strained ZnSe-rich layer at the barrier-QD interface. An ultrathin pseudomorphic ZnSe-rich layer forms at the QD-barrier interface due to desorption of Cd and due to

the preferential Zn incorporation [29] during MEE [20]. Nevertheless, this interfacial layer does not interfere with the hole confinement levels within the QDs due to a large VB offset [15]

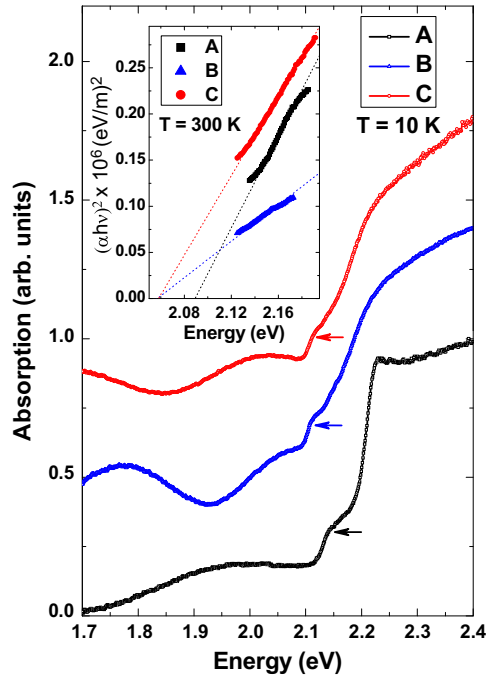


**Fig. 2.** Results from absorption measurements. The plot of normalized absorption for the three samples taken at 10 K. Arrows indicate enhanced below band gap absorption due to presence of ZnTe QDs. Inset: the plot of  $(\alpha h\nu)^2$  vs. photon energy at room temperature, the data points are fitted with a straight line to obtain the band edges.

between ZnTe and ZnSe, in contrast to the effect that would have been produced by a ZnTe wetting layer.

We further performed HRXRD based reciprocal space mapping on sample A to investigate the vertical correlation of the QDs. The vertical correlation is important in order to ensure sufficient overlap of the QD confined hole wave functions to facilitate the miniband formation [30–33] within the band gap of the ZnCdSe host. The difference in the scattering factors of the QD material and the matrix as well as the elastic deformation strain field in the matrix surrounding the QDs cause diffuse scattering to appear in the reciprocal space map (RSM) along with the coherent scattering [28,34]. A theoretical description based on a statistical kinematical approach showed that the diffuse scattering around the coherent SL peaks gets elongated along the  $x$ -component of the momentum transfer ( $q_x$ ) if the QDs are vertically correlated [34]. Fig. 3 (b) shows the RSM along (002) reflection, while the diffuse scattered intensity around the first order SL peak is shown in Fig. 3(c). The diffuse scattered intensity is found to be elongated along the  $q_x$  direction indicating a vertical correlation of the dots within the multilayer structure. From the widths of the diffuse maxima ( $\delta q_z$ ) along the  $z$ -component of the momentum transfer ( $q_z$ ) (see Fig. 3(d)), we determined that the degree of vertical correlation [34] ( $\xi_{ver} \approx 2\pi/\delta q_z$ ) is roughly 0.4, hence approximately 40% QDs are correlated vertically along the growth direction forming stacks of QDs. The vertical QD alignment obtained in case of this sample is supposed to give rise to the uniformity in QD size, improving the structural quality and consequently overall IB-SC performance [35]. Additionally, the stacked QDs are expected to facilitate the formation of a miniband due to very thin barriers, leading to formation of an IB within the bandgap of ZnCdSe, the basis of the working principle of the IB-SC concept.

Having obtained the structural information from HRXRD along with absorption data and confirming the parameters using simulations, a typical band line-up for this material system at room

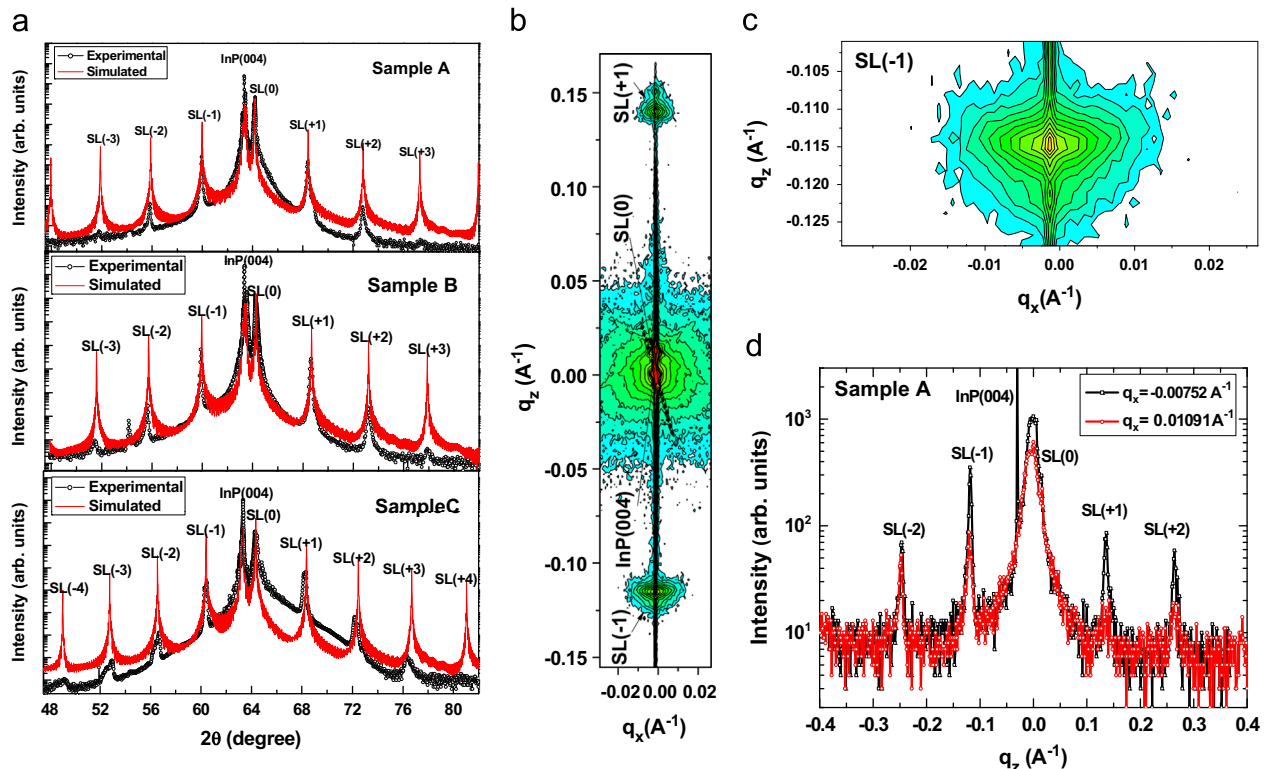


**Fig. 3.** Structural analysis of QD multilayer SLs. (a) Experimental and simulated  $\omega$ - $2\theta$  curves for samples A, B, and C along (004) reflection showing multiple satellite SL peaks. (b) RSM of sample A along (002) reflection. (c) Enlarged RSM around first order satellite SL peak showing clear elongation of diffuse scattering along  $q_x$  direction. (d)  $q_z$  scans for two non-zero values of  $q_x$  measured in order to estimate  $\delta q_z$ .

**Table 1**  
Summary of the important parameters calculated using HRXRD and absorption measurements along with those obtained from the simulations.

Sample	Buffer layer composition	Barrier composition		Barrier band edge in eV	SL period in nm
		Experimental	Simulated		
A	Zn <sub>0.49</sub> Cd <sub>0.51</sub> Se	Zn <sub>0.49</sub> Cd <sub>0.51</sub> Se	Zn <sub>0.49</sub> Cd <sub>0.51</sub> Se <sub>0.99</sub> Te <sub>0.01</sub>	2.09	2.38
B	Zn <sub>0.49</sub> Cd <sub>0.51</sub> Se	Zn <sub>0.49</sub> Cd <sub>0.51</sub> Se <sub>0.975</sub> Te <sub>0.025</sub>	Zn <sub>0.49</sub> Cd <sub>0.51</sub> Se <sub>0.976</sub> Te <sub>0.024</sub>	2.06	2.36
C	Zn <sub>0.50</sub> Cd <sub>0.50</sub> Se	Zn <sub>0.50</sub> Cd <sub>0.50</sub> Se <sub>0.970</sub> Te <sub>0.030</sub>	Zn <sub>0.50</sub> Cd <sub>0.50</sub> Se <sub>0.973</sub> Te <sub>0.027</sub>	2.06	2.64

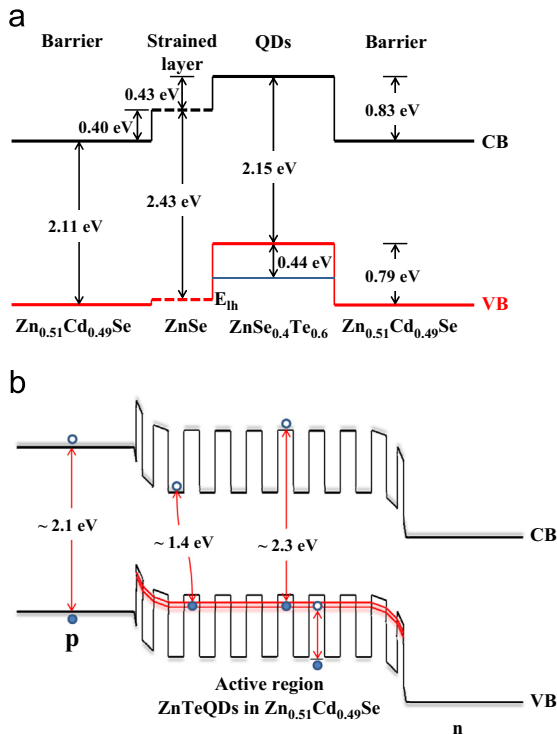


**Fig. 4.** Typical band line-up and proposed IB-SC structure. (a) The calculated band line-up diagram at room temperature for the system under investigation. Here,  $E_{lh}$  is the energy level of light hole in ZnSe, shown with a dotted line. Also, the ground state for holes within 0.5 nm thick ZnTe QD is shown with a blue line. (b) The band line-up for proposed IB solar cell p-i-n structure at room temperature, comprising ~1.2 nm thick ZnTe QDs embedded in ZnCdSe matrix as an active layer. (For interpretation of the references to color in this figure legend, the reader is referred to the web version of this article.)

temperature is calculated and is shown in Fig. 4(a). The band gaps and band offsets used for the calculation are those corresponding to the perfectly lattice matched Zn<sub>x</sub>Cd<sub>1-x</sub>Se barriers [14,15,26,36] and fully relaxed ZnSe<sub>0.4</sub>Te<sub>0.6</sub> QDs [15,26,37,38]. The thickness (height) of the QDs was assumed to be ~0.5 nm in order to calculate the hole confinement energy level within the ZnTe QD [15–17,26] using the 1-dimensional Schrodinger equation that are in agreement with the PL and absorption peak positions. The modification in the energy levels due to in-plane confinement can be neglected supposing the QD radius of ~10 nm, as obtained previously for similarly grown samples [39]. The energy levels of a heavy hole and a light hole were calculated for a completely strained ZnSe layer using known values of the deformation potentials and the elastic constants [40].

Additionally, the calculations demonstrate that an IB can in principle be engineered at ~0.7 eV from the hole confinement levels within 1.2 nm thick ZnTe QDs, which can be achieved by using higher Te fluxes during the growth and by carefully calibrating them to get required QD thicknesses. Based on the experimental results and performed calculations, we propose here an IB-SC p-i-n structure with ~1.2 nm thick ZnTe QDs in the

active region as shown in Fig. 4(b), while fabrication of an active device with these optimized parameters is underway. The possible transitions, including those which would initiate below band gap absorption due to formation of IB are shown by the arrows.

## 5. Summary

In summary, we have grown multilayer structures containing submonolayer ZnTe-rich QDs embedded in ZnCdSe with 150 periods without formation of wetting layers using MEE. The host was engineered to be lattice matched to the InP substrate as well as to have close to optimal host bandgap predicted for an ideal IB-SC. The vertical correlation of the QDs demonstrated the possibility of IB formation, which in turn contributed to the absorption of photons with energies below the host bandgap. Moreover, the QDs were shown to be of type-II in nature, which is expected to suppress the non-radiative Auger recombination as well as to improve carrier extraction. A typical band alignment of the proposed proto-type multilayer ZnTe/ZnCdSe QD structure with optimal parameters is presented. The physical and material properties of the proposed structure are believed to be the best possible match to an active material for a working IB-SC; thus expected to enhance the short circuit current while preserving the open circuit voltage when incorporated in a photovoltaic device.

## Acknowledgments

This research was supported by the Department of Energy, Office of Basic Energy Sciences, Division of Materials Sciences and Engineering under Award No. SC003739. Use of the National Synchrotron Light Source, Brookhaven National Laboratory, was supported by the U.S. Department of Energy, Office of Science, Office of Basic Energy Sciences, under Contract No. DE-AC02-98CH10886. One of us (RM) acknowledges support from the NSF-CREST CENSES under Award no. HRD0833180.

## References

- [1] A. Luque, A. Martí, Increasing the efficiency of ideal solar cells by photon induced transitions at intermediate levels, *Physical Review Letters* 78 (1997) 5014–5017.
- [2] W. Shockley, H.J. Queisser, Detailed balance limit of efficiency of p-n junction solar cells, *Journal of Applied Physics* 32 (1961) 5105–5119.
- [3] G.L. Araújo, A. Martí, Absolute limiting efficiencies for photovoltaic energy conversion, *Solar Energy Materials and Solar Cells* 33 (1994) 213–240.
- [4] A. Luque, A. Martí, The intermediate band solar cell: progress toward the realization of an attractive concept, *Advanced Materials*, 22, 160–174.
- [5] A. Luque, A. Martí, C. Stanley, Understanding intermediate-band solar cells, *Nature Photon* 6 (2012) 146–152.
- [6] A. Luque, A. Martí, N. López, E. Antolín, E. Cánovas, C. Stanley, et al., Experimental analysis of the quasi-Fermi level split in quantum dot intermediate-band solar cells, *Applied Physics Letters* (2005) 083505-1–083505-3.
- [7] A. Martí, E. Antolín, C. Stanley, C. Farmer, N. López, P. Díaz, et al., Production of photocurrent due to intermediate-to-conduction-band transitions: a demonstration of a key operating principle of the intermediate-band solar cell, *Physical Review Letters* 97 (2006) 247701-1–247701-4.

- [8] K. Sablon, J. Little, V. Mitin, A. Sergeev, N. Vagidov, K. Reinhardt, Strong enhancement of solar cell efficiency due to quantum dots with built-in charge, *Nano Letters* 11 (2011) 2311–2317.
- [9] Q. Shao, A.A. Balandin, A.I. Fedoseyev, M. Turowski, Intermediate-band solar cells based on quantum dot supracrystals, *Applied Physics Letters* 91 (2007) 163503-1–163503-3.
- [10] V. Popescu, A. Zunger, Three-dimensional assemblies of semiconductor quantum dots in a wide-gap matrix providing an intermediate band for absorption, *Journal of Applied Physics* 112 (2012) 114320-1–114320-10.
- [11] A. Martí, N. López, E. Antolín, E. Cánovas, A. Luque, C.R. Stanley, et al., Emitter degradation in quantum dot intermediate band solar cells, *Applied Physics Letters* 90 (2007) 233510-1–233510-3.
- [12] A.M. Kechiantz, L.M. Kocharyan, H.M. Kechiyants, Band alignment and conversion efficiency in Si/Ge type-II quantum dot intermediate band solar cells, *Nanotechnology* 18 (2007) 405401-1–405401-12.
- [13] P.G. Linares, A. Martí, E. Antolín, C.D. Farmer, Í. Ramiro, C.R. Stanley, et al., Voltage recovery in intermediate band solar cells, *Solar Energy Materials and Solar Cells* 98 (2012) 240–244.
- [14] Y.D. Kim, M.V. Klein, S.F. Ren, Y.C. Chang, H. Luo, N. Samarth, et al., Optical properties of zinc-blende CdSe and Zn<sub>x</sub>Cd<sub>1-x</sub>Se films grown on GaAs, *Physical Review B* 49 (1994) 7262–7270.
- [15] W. Faschinger, S. Ferreira, H. Sitter, Doping of zinc-selenide-telluride, *Applied Physics Letters* 64 (1994) 2682–2684.
- [16] J. Puls, M. Rabe, H.-J. Wunsche, F. Henneberger, Magneto-optical study of the exciton fine structure in self-assembled CdSe quantum dots, *Physical Review B* 60 (1999) R16303–R16306.
- [17] D.J. Milliron, S.M. Hughes, Y. Cui, L. Manna, Colloidal nanocrystal heterostructures with linear and branched topology, *Nature* 430 (2004) 190–195.
- [18] G.G. Zegrya, A.D. Andreev, Mechanism of suppression of Auger recombination processes in type-II heterostructures, *Applied Physics Letters* 67 (1995) 2681–2683.
- [19] H. Zhu, N. Song, W. Rodríguez-Córdoba, T. Lian, Wave function engineering for efficient extraction of up to nineteen electrons from one CdSe/CdS quasi-type II quantum dot, *Journal of the American Chemical Society* 134 (2012) 4250–4257.
- [20] S. Dhomkar, I.L. Kuskovsky, U. Manna, I.C. Noyan, M.C. Tamargo, Optimization of growth conditions of type-II Zn(Cd)Te/ZnCdSe submonolayer quantum dot superlattices for intermediate band solar cells, *Journal of Vacuum Science and Technology B* 31 (2013) 03C119-1–03C119-7.
- [21] Y. Gu, I.L. Kuskovsky, M. van der Voort, G.F. Neumark, X. Zhou, M.C. Tamargo, Zn–Se–Te multilayers with submonolayer quantities of Te: type-II quantum structures and isoelectronic centers, *Physical Review B* 71 (2005) 045340-1–045340-4.
- [22] I.L. Kuskovsky, Y. Gu, Y. Gong, H.F. Yan, J. Lau, I.C. Noyan, et al., Mechanism for increasing dopant incorporation in semiconductors via doped nanostructures, *Physical Review B* 73 (2006) 195306-1–195306-5.
- [23] W. Lin, S.P. Guo, M.C. Tamargo, I. Kuskovsky, C. Tian, G.F. Neumark, Enhancement of p-type doping of ZnSe using a modified (N+Te) $\delta$ -doping technique, *Applied Physics Letters* 76 (2000) 2205–2207.
- [24] N.N. Ledentsov, J. Böhrer, M. Beer, F. Heinrichsdorff, M. Grundmann, D. Bimberg, et al., Radiative states in type-II GaSb/GaAs quantum wells, *Physical Review B* 52 (1995) 14058–14066.
- [25] F. Hatami, M. Grundmann, N.N. Ledentsov, F. Heinrichsdorff, R. Heitz, J. Böhrer, et al., Carrier dynamics in type-II GaSb/GaAs quantum dots, *Physical Review B* 57 (1998) 4635–4641.
- [26] V.A. Shuvayev, I.L. Kuskovsky, L.I. Deych, Y. Gu, Y. Gong, G.F. Neumark, et al., Dynamics of the radiative recombination in cylindrical nanostructures with type-II band alignment, *Physical Review B* 79 (2009) 115307-1–115307-9.
- [27] Y. Gong, H.F. Yan, I.L. Kuskovsky, Y. Gu, I.C. Noyan, G.F. Neumark, et al., Structure of Zn–Se–Te system with submonolayer insertion of ZnTe grown by migration enhanced epitaxy, *Journal of Applied Physics* 99 (2006) 064913-1–064913-5.
- [28] U. Manna, I.C. Noyan, Q. Zhang, I.F. Salakhutdinov, K.A. Dunn, S.W. Novak, et al., Structural properties and spatial ordering in multilayered ZnMgTe/ZnSe type-II quantum dot structures, *Journal of Applied Physics* 111 (2012) 033516-1–033516-7.
- [29] T. Passow, H. Heinke, T. Schmidt, J. Falta, a. Stockmann, H. Selke, et al., Segregation-enhanced etching of Cd during Zn deposition on CdSe quantum dots, *Physical Review B* 64 (2001) 193311-1–193311-4.
- [30] N.N. Ledentsov, V.A. Shchukin, M. Grundmann, N. Kirstaedter, J. Böhrer, O. Schmidt, et al., Direct formation of vertically coupled quantum dots in Stranski–Krastanow growth, *Physical Review B* 54 (1996) 8743–8750.
- [31] O.L. Lazarenkova, A.A. Balandin, Miniband formation in a quantum dot crystal, *Journal of Applied Physics* 89 (2001) 5509–5515.
- [32] O.L. Lazarenkova, A.A. Balandin, Electron and phonon energy spectra in a three-dimensional regimented quantum dot superlattice, *Physical Review B* 66 (2002) 245319-1–245319-9.
- [33] D. Nika, E. Pokatilov, Q. Shao, A. Balandin, Charge-carrier states and light absorption in ordered quantum dot superlattices, *Physical Review B* 76 (2007) 125417-1–125417-9.
- [34] A.A. Darhuber, P. Schittenhelm, V. Holý, J. Stangl, G. Bauer, G. Abstreiter, High-resolution X-ray diffraction from multilayered self-assembled Ge dots, *Physical Review B* 55 (1997) 15652–15663.
- [35] W. Liu, H. Wu, F. Tsao, T. Hsu, J. Chyi, Improving the characteristics of intermediate-band solar cell devices using a vertically aligned InAs/GaAsSb quantum dot structure, *Solar Energy Materials and Solar Cells* 105 (2012) 237–241.
- [36] E. Tyrrell, J. Smith, Effective mass modeling of excitons in type-II quantum dot heterostructures, *Physical Review B* 84 (2011) 165328-1–165328-12.
- [37] S. Adachi, T. Taguchi, Optical properties of ZnSe, *Physical Review B* 43 (1991) 9569–9577.
- [38] K. Sato, S. Adachi, Optical properties of ZnTe, *Journal of Applied Physics* 73 (1993) 926–931.
- [39] B. Roy, H. Ji, S. Dhomkar, F.J. Cadieu, L. Peng, R. Moug, et al., Determination of excitonic size with sub-nanometer precision via excitonic Aharonov–Bohm effect in type-II quantum dots, *Applied Physics Letters* 100 (2012) 213114-1–213114-3.
- [40] C.G. Van de Walle, Band lineups and deformation potentials in model-solid theory, *Physical Review B* 39 (1989) 1871–1883.